Available online at www.sciencedirect.com
SCIENCE DIRECT®
Electrochimica Acta 50 (2005) 1113–1119
ELECTROCHIMICA Acta
www.elsevier.com/locate/electacta

Electron transfer across anodic films formed on tin in carbonate-bicarbonate buffer solution

C.A. Gervasi[a,b,*], M.E. Folquer[c], A.E. Vallejo[b], P.E. Alvarez[d]

[a] *Instituto de Investigaciones Fisicoquímicas Teóricas y Aplicadas (INIFTA), Facultad de Ciencias Exactas, Universidad Nacional de La Plata, Sucursal 4, C.C. 16, (1900) La Plata, Argentina*
[b] *Laboratorio de Ingeniería de Corrosión y Tecnología Electroquímica (LICTE), Facultad de Ingeniería, Universidad Nacional de La Plata, 1 y 47, (1900) La Plata, Argentina*
[c] *Instituto de Química Física, Facultad de Bioquímica, Química y Farmacia, Universidad Nacional de Tucumán, Ayacucho 471, (4000) Tucumán, Argentina*
[d] *Instituto de Física, Facultad de Bioquímica, Química y Farmacia, Universidad Nacional de Tucumán, Ayacucho 471, (4000) Tucumán, Argentina*

Received 26 April 2004; received in revised form 14 July 2004; accepted 7 August 2004
Available online 11 September 2004

Abstract

Impedance and steady-state data were recorded in order to study the kinetics of electron transfer between passive tin electrodes and an electrolytic solution containing the $K_3Fe(CN)_6$–$K_4Fe(CN)_6$ redox couple. Film thickness plays a key role in determining the type of electronic conduction of these oxide covered electrodes. Electron exchange with the oxide takes place with participation of the conduction band in the semiconducting film. A mechanism involving direct electron tunneling through the space charge barrier is the most suitable to interpret the experimental evidence.

Keywords: Tin; Anodic oxide films; Electronic conduction; Electron transfer reaction; Impedance spectroscopy

1. Introduction

Passivation of tin in carbonate-bicarbonate buffers has been considered in several works, since within the pH range of these electrolytes the solubility of various tin oxide-hydroxides is comparatively low [1–3]. The oxidation of tin in solutions of pH around 8.5 could theoretically give rise to the formation of stannous hydroxide. A greater degree of oxidation leads to the formation of stannic hydroxide. Both hydroxides are thermodynamically less stable than the corresponding oxides SnO and SnO_2, and tend to change into these oxides. The oxide SnO is usually not present in large amounts, on account of its instability in relation to Sn and SnO_2. In actual fact, in near neutral media the metal can be oxidized directly to stannic oxide. Moreover stannic hydroxide soon dehydrates into SnO_2. Thus, the passive film is usually described as composed of hydroxides and oxides with SnO_2 as the predominant species [4].

In principle, a corrosion reaction is a redox reaction of the metal, where the reaction of the available oxidant in solution consumes the electrons transported through the oxide. Consequently, not only ion transport processes but electron transport across the film can play a fundamental role in corrosion kinetics. Hence, it is relevant to this field to present information relating to the electronic properties of passive films [5–7]. Furthermore, gaining an insight into the electronic structure of oxide films and the electrical properties of the oxide/electrolyte interface is also relevant to microelectronics and optical film semiconductor technology. The interest in considering SnO_2 thin films lies in its use as electrodes and semitransparent conductive arrays [8]. Capacitance studies

* Corresponding author. Tel.: +54 221 425 7430; fax: +54 221 425 4642.

0013-4686/$ – see front matter © 2004 Elsevier Ltd. All rights reserved.
doi:10.1016/j.electacta.2004.08.008

of the semiconducting properties of passive films anodically grown on tin in borate buffer solutions confirmed that the electronic structure of the passive film is similar to that of bulk SnO_2 [9]. The presence of recombination centers within the space charge region has been postulated to explain the photoresponse of these electrodes [10]. Metikoš-Huković et al. used impedance spectroscopy and cyclic voltammetry measurements to examine solid-state properties of thin anodic films on tin. A change of slope in Mott-Schottky plots was ascribed to partial ionization of deep-level electronic states [11].

Film thickness is a key factor in determining the mechanism for electron transfer reactions (ETR) that take place on passive layers. For very thin films, direct tunneling from the metal represents the main contribution to electron transfer and an increase in thickness results in increased tunneling distance and exponentially decreased tunnel probability [12]. On the other hand, ETR on thick films take place as on semiconductor electrodes, with participation of electronic states in the band gap. Steady-state polarization curves were used to study the kinetics of charge transfer between passive tin electrodes and $K_3Fe(CN)_6$–$K_4Fe(CN)_6$ redox couple in borate buffer solutions. The behavior ranges from almost metallic, for very thin films, to that of an *n*-type semiconductor, for thick films [13]. It is noteworthy that the rate of ETR depends not only on the type of metal, but also on the preparation of the oxide film, which determines its thickness and the concentration of donors or acceptors.

Electrochemical impedance spectroscopy (EIS) is a powerful tool to study not only electronic properties of passive films but mechanisms of electron transfer reactions, as well. However, at present this technique has not been applied to characterize ETR on passive tin electrodes.

The main objective of this work is to present experimental results that enable one to gain a deeper insight into the mechanisms of electron transfer at oxide covered tin electrodes obtained in carbonate-bicarbonate solution. Consequently, polarization curves and impedance spectra were recorded for tin electrodes passivated in 0.75 M $KHCO_3$ + 0.05 M K_2CO_3 buffer solution pH 8.9 and in the presence of the $K_3Fe(CN)_6$–$K_4Fe(CN)_6$ redox couple.

2. Experimental

The experimental set-up was described in previous publications [3]. “Specpure” tin in the form of both static and rotating discs (Johnson Matthey Chemical Ltd., 0.30 cm^2 apparent area) axially mounted in PTFE holders were used as working electrodes. The exposed tin surface was polished to a mirror finish with 1.0 and 0.3 μm alumina powder, rinsed in triply distilled water and held 5 min at potentials sufficiently negative to produce a net hydrogen evolution. The counter electrode was a large area Pt sheet. Potentials were measured and referred to in the text against a saturated calomel electrode (SCE) (0.242 V in the SHE scale).

Experiments were made under purified N_2 gas saturation at 25 °C. Tin electrodes were anodised in 0.75 M $KHCO_3$ + 0.05 M K_2CO_3 solution pH 8.9. The electrolyte was prepared from analytical grade (p.a. Merck) chemicals and triply distilled water.

Films were anodically grown for 7 h at constant potential E_f ($-0.1\,V \leq E_f \leq 2.0\,V$) set within the passivity region, in carbonate-bicarbonate buffer solution, which was thereafter replaced by the redox solution. The redox system used was 0.05 M $K_3Fe(CN)_6$–$K_4Fe(CN)_6$ dissolved in 0.75 M $KHCO_3$ + 0.05 M K_2CO_3 buffer solution, pH 8.9.

Polarization curves for films grown at different E_f were measured in the redox solution, under steady-state conditions, using a rotating disk electrode to eliminate diffusion effects.

EIS data were measured with a Solartron SI 1254 device; a 10 mV amplitude sine-wave signal perturbation was applied in a wide frequency range. Impedance spectra were obtained at the formation potential, E_f ($-0.1\,V \leq E_f \leq 2.0\,V$) selected within the passivity region. Additionally, for oxides with different thicknesses impedance spectra were recorded in the solution containing the redox couple, applying three different polarization levels, namely, the equilibrium potential, 150 mV anodic overpotential and −150 mV cathodic overpotential.

3. Results and discussion

3.1. Band structure of the passive film

An interpretation of ETR that take place on the passive film requires first to derive the band structure of the oxide.

In order to characterize both the electronic properties of the anodic film and the influence of E_f on these properties, EIS measurements were performed at different potentials within the passivity range of the system under study. Fig. 1 shows Nyquist and Bode plots obtained at E_f = 0.0, 0.4 and 0.8 V.

According to the processes taking place in the metal/oxide/solution system, the total current I is the sum of I_{ec}, the electronic current due to the transport of electrons and/or holes, and I_i, the ionic current due to the transport of ions or vacancies through the film. In this work these currents are considered to be independent of one another, so that $I = I_{ec} + I_i$. When no redox reactions take place, the electronic current only involves the charging processes of the different interfacial capacitances, namely the space charge capacitance due to shallow levels and the capacitance of a mid-bandgap electronic state, both in the oxide film, and the Helmholtz layer capacitance in the solution. Accordingly, in the model applied to describe the experimental data the impedance due to these non-faradaic processes (Z_{ec}) results in parallel with the impedance of the ionic transport in the oxide (Z_i).

$$\frac{1}{Z_T} = \frac{1}{Z_i} + \frac{1}{Z_{ec}} \quad (1)$$

where Z_T is the total impedance function.

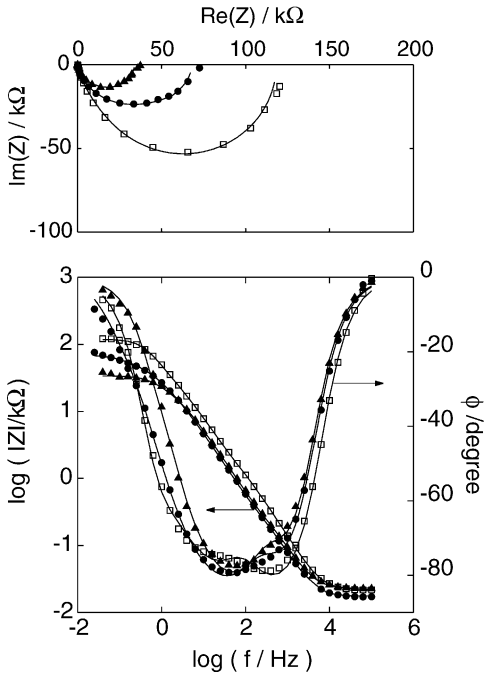

Fig. 1. Nyquist and Bode plots of experimental impedance data for passivated tin electrodes in 0.75 M $KHCO_3$ + 0.05 M K_2CO_3, pH 8.9, for different formation potentials, E_f = 0 V (▲); E_f = 0.4 V (●) and E_f = 0.8 V (□). Fit results according to Eq. (1) (—).

The expression of Z_i, as previously derived, is based on the physicochemical processes that occur within a passive film according to the Point Defect Model [14–16]. Thus, solving the high-field transport equation introduced by Fromhold and Cook [17,18] with boundary conditions reflecting the charge transfer reactions at the metal/oxide and oxide/solution interfaces yields an expression for Z_i that allows to estimate the diffusion coefficient of ionic defects D and the film thickness L. Derivation of this equation and its success in describing experimental data was discussed in a previous work [19]. Since Z_i dominates the low frequency portion of the impedance spectra and so, it is not related to the electronic processes in the film, no further analysis will be presented here. However, it is worth to mention that the followed fitting procedure, according to the global impedance expression below, involves non-linear least squares and the yielded parameter estimates are associated with *all* data, rather than with a portion for a given frequency range. This procedure provides uncertainty estimates for all estimated parameters, showing that all parameters are relevant in the model.

At high frequencies the impedance becomes increasingly dominated by the Z_{ec} component related to the capacitance of the depletion layer (C_{sc}) in the oxide and the occurrence of electronic states in the forbidden gap, at the surface (surface states) or distributed within the bulk of the material (C_{ss}). The classical approach to represent Z_{ec} is based on the equivalent circuit shown in Fig. 2. This electrical analog can be applied to characterize the effect of either bulk or surface deep-level species [20]. This model was adopted here, since

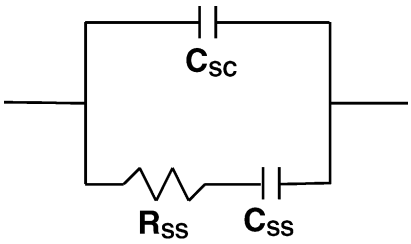

Fig. 2. Equivalent circuit corresponding to the impedance due to non-faradaic processes Z_e. Circuit elements represent the capacitance of the depletion layer in the oxide (C_{sc}) and a time constant associated with electronic states in the band gap ($C_{ss}R_{ss}$). Values of circuit elements are independent of frequency but are functions of potential.

every attempt to fit the experimental results to a simple series RC circuit (containing solely the capacitance C_{sc}) results in frequency dispersion phenomena for the capacitance data, indicating that additional capacitance elements are present in the interfacial region [21]. Physically this could arise from various modes of inhomogeneous charge accumulation, like deep traps or surface states.

Experimental impedance spectra were fitted according to Eq. (1) and the corresponding fit results can be observed in Fig. 1. Good agreement between theory and experiment was obtained for the whole frequency range.

The space-charge capacitance (C_{sc}) values resulting from the fitting procedure are shown in Fig. 3 as Mott-Schottky plots. A linear relationship was obtained for $E_f \geq 0.4$ V, which corresponds to a *n*-type semiconductor film and verifies the existence of a true depletion layer. The extrapolated flat band potential $E_{fb} = -0.176$ V for the film formed at 0.4 V, is in excellent agreement with previously reported results of tin oxides electroformed at E_f = 0.4 V in 0.2 M NaOH solution [22]. Assuming a value for the dielectric constant ε = 15 [22,23], the slope of the Mott-Schottky plot yields a donor concentration value $N_d = 2.53 \times 10^{20}$ cm^{-3}, which is somewhat larger than the one reported in Ref. [22], but it is still within the typical range of doping level obtained for most passive films. Calculated values of N_d, and E_{fb}, for E_f = 0.4 and 0.8 V, are shown in Table 1.

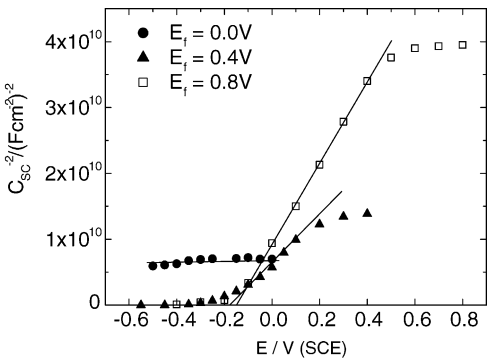

Fig. 3. Mott-Schottky plots for space-charge capacitance (C_{sc}) values derived from the fit of experimental impedance spectra that were recorded for films grown at different E_f.

Table 1
Slope of the Mott-Schottky plot, concentration of donor levels (N_D), flat-band potential (E_{FB}) and maximum width of the space charge layer W_{max} calculated from data presented in Fig. 3 and Eq. (2)

E_f (V)	Slope (F/cm^4 V)	N_D (cm^{-3})	E_{FB} (V)	W_{max} (nm)	L (nm)
0	–	–	–	–	2.05
0.4	3.71×10^{10}	2.53×10^{20}	−0.176	2.0	3.94
0.8	6.22×10^{10}	1.51×10^{20}	−0.147	3.2	5.44

Film thickness L derived from the fitting procedure applied to impedance data.

For $E_f = 0$ V C_{sc} values are independent of the applied potential (Fig. 3). Moreover, since these values, after correction for the surface roughness, result considerably lower than typical values for the capacitance of the double layer, it is clear that the oxide does not exhibit metallic conductivity. Thus, following the accepted explanation in the relevant literature, a constant capacitance can be interpreted in terms of an oxide depleted of charge carriers, as experimentally found for passive films on iron [24]. It can be theoretically shown that the film becomes increasingly exhausted upon increasing potential and acts as an insulator. For the particular case where the thickness of the space charge layer equals the film thickness, the film becomes completely exhausted and behaves as an insulator in the whole potential range [25,26]. Therefore, the capacitance is that of a parallel-plate capacitor with a plate separation equal to the oxide thickness L. An experimental confirmation that this conditions prevail in our experiments for the film formed at $E = 0$ V, can be obtained by comparing the maximum thickness of the space charge layer, obtained in the range of validity of the Mott-Schottky equation for a semiconductor film (Eq. (2) below) and L values as previously determined from Z_i in impedance measurements and the charge density for the electroreduction of the passive films [19].

The maximum thickness for the space charge layer W_{max} corresponds to a polarization level $E = E_f$ and can be written as:

$$W_{max} = \left(\frac{2\varepsilon\varepsilon_0 |E_f - E_{fb}|}{qN_d} \right)^{1/2} \quad (2)$$

where ε_0 is the permittivity of free space and q the electron charge.

Values of W_{max} and L derived for the oxide films in Fig. 3 are presented in Table 1.

The dielectric properties of the insulating oxide film can be examined in terms of the model for a parallel-plate capacitor, to calculate a roughness factor, Υ, according to:

$$\Upsilon = \frac{LC_{SC}}{\varepsilon\varepsilon_0} \approx 2.0 \frac{\text{cm}^2}{\text{cm}^2_{ap}} \quad (3)$$

with $L = 2.05$ nm and $C_{sc} = 1.2 \times 10^{-5}$ cm$^{-2}_{ap}$ as results from the fitting procedure, $\varepsilon = 15$ and $\varepsilon_0 = 8.85419 \times 10^{-14}$ coul V^{-1} cm^{-1}.

This value of Υ agrees well with that, estimated from capacitance measurements, for mechanically polished tin electrodes anodised in borate solution pH 8.5 [27].

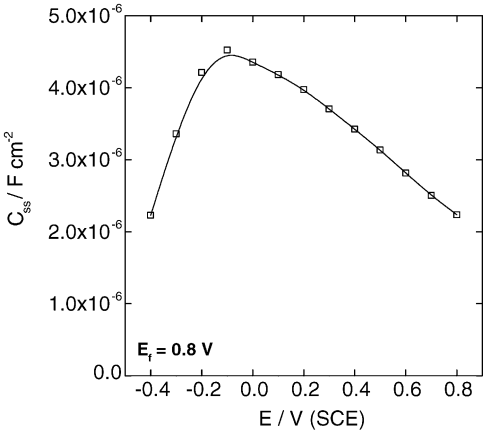

Fig. 4. Potential dependence of C_{ss} for passive tin films grown at $E_f = 0.8$ V.

The applied potential can be used as a probe to resolve the spatial distribution of deep electronic states within the band gap, through the analysis of the potential dependence of C_{ss} [20,28]. Results for passive films grown at $E_f = 0.8$ V are presented Fig. 4. In principle, the presence of a maximum in this plot might indicate the presence of electronic states that are mainly located at the surface [29,30]. However, the presented experimental evidence is insufficient to completely rule out the presence of additional deep electronic states in the bulk of the semiconducting oxide. From the band-structure point of view, one may state that the density of states does not go to zero at the conduction band edge, at least at the surface.

Due to its amorphous nature, oxide films formed by anodic passivation lack long-range order, with band edges that are not sharply defined. However, bulk semiconductor models considered so far, were proved to be still applicable to describe passive films [31].

3.2. Electron transfer reactions (ETR)

Rates of electron transfer across passive films are slower than on bare metals, reflecting semiconducting properties. The decrease in the rate constant depends strongly on film thickness, composition and type of conductivity. Likewise, reaction rates are also dependent on the relative position of the redox potential E_{rdx} and E_{fb} [32].

The redox potential for passive tin electrodes was established in the solution containing the redox couple, reaching the same value as on Pt ($E_{rdx} = 0.210$ V), after 5 min for films formed at $E_f \leq 1.0$ V and after 1 h for thicker films. This behavior is usually observed on passive metal electrodes.

Steady-state currents for the redox couple were measured at constant overpotential (η) and varying the rotation speed (w) between 600 and 3000 rpm. These currents were recorded within 5 min (typically 30 s) after imposing a potential step. At each η, extrapolating current values to infinite rotation speed allowed us to eliminate mass transport effects and to calculate the kinetic component of the measured current density (j_k).

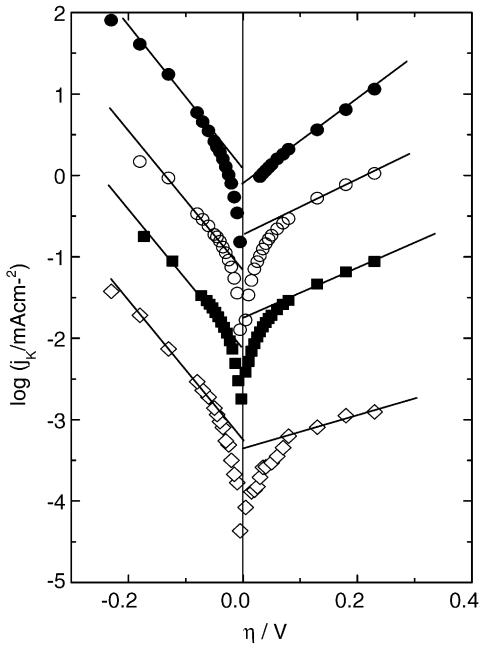

Fig. 5. Polarization curves for the redox system $K_3Fe(CN)_6$–$K_4Fe(CN)_6$ on passive tin electrodes. Passive films were grown at different formation potentials, E_f = 0.5 V (●); E_f = 1.0 V (○); E_f = 1.5 V (■) and E_f = 2.0 V (◇).

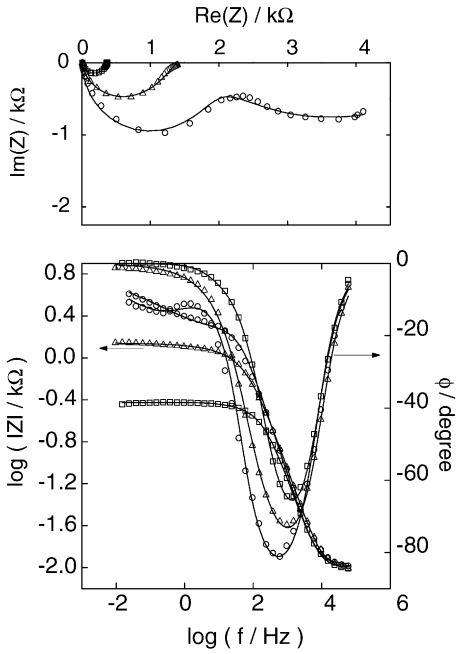

Fig. 6. Experimental impedance spectra for tin electrodes passivated at E_f = 1.5 V in the presence of the redox system $K_3Fe(CN)_6$–$K_4Fe(CN)_6$. Impedance data were recorded at η = 0 V (○), + 0.15 V (△) and −0.15 V (□).

Fig. 5 shows polarization curves (j_k versus η) for tin electrodes that were previously passivated within the 0.5–2.0 V range in order to vary at convenience the film thickness. It was observed that the exchange current density j_o decreases strongly with increasing film thickness. In all cases j_o values result much smaller than those measured on Pt under similar conditions ($j_{o/Pt}$ = 0.1 A cm^{-2}).

Anodic and cathodic branches of the polarization curves at each potential E_f are asymmetric, according to unequal transfer coefficient (α) values. Transfer coefficients for the cathodic Tafel regions (α_-) are close to 0.5. On the other hand, anodic transfer coefficients (α_+) decrease with film thickness from 0.31 to 0.12. Thus, the anodic reaction becomes increasingly blocked for increasing E_f, as expected for an *n*-type semiconductor. On the whole, these results reflect an increasing semiconducting character for thicker films. Results are summarized in Table 2.

Fig. 6 shows impedance data as Nyquist and Bode plots corresponding to a film formed at E_f = 1.5 V that were recorded at E_{rdx} and at two polarization levels within the Tafel regions for the redox couple, namely, η = 0 V, +0.15 and −0.15 V. Electrodes were rotated at $w = 2000$ rpm to avoid mass transport effects in solution.

In the presence of a redox couple in solution, the electronic current results from the sum of the electronic transfer (I_{rr}), due to the redox reaction, and the displacement current (I_{ec}), due to charging processes of the different interfacial capacitances. Consequently, the impedance due to non-faradaic processes (Z_{ec}) results in parallel with the impedance of ionic transport in the oxide (Z_i) and the impedance of electronic transfer (Z_{rr}) [33]:

$$\frac{1}{Z_T} = \frac{1}{Z_i} + \frac{1}{Z_{ec}} + \frac{1}{Z_{rr}} \tag{4}$$

Eq. (4) represents an extension of Eq. (1) to account for a redox electrolyte.

Moreover, when mass transport effects are negligible Z_{rr} has a purely resistive behavior and $Z_{rr}(\omega) = R_{rr}$.

Best-fit results according to Eq. (4) are presented in Fig. 6. At the equilibrium potential it is possible to calculate j_o values in a simple way, by using the values of R_{rr} derived from the fitting procedure:

$$j_o = \left(\frac{RT}{F}\right)\frac{1}{R_{rr}}\bigg|_{E=E_{rdx}} \tag{5}$$

Table 2
Kinetic parameters of the $Fe(CN)_6^{3-}/Fe(CN)_6^{4-}$ redox reaction on passive tin electrodes obtained by EIS and steady-state polarization curves for different E_f

E_f (V)	α_+ (EIS)	α_+ (steady-state data)	α_- (EIS)	α_- (steady-state data)	j_o (mA cm^{-2}) (EIS)	j_o (mA cm^{-2}) (steady-state data)
0.5	0.36	0.31	0.47	0.50	0.554	0.575
1.0	0.25	0.20	0.45	0.48	0.087	0.060
1.5	0.29	0.18	0.47	0.49	7.72×10^{-3}	6.04×10^{-3}
2.0	0.22	0.12	0.52	0.50	2.18×10^{-4}	2.27×10^{-4}

Likewise, R_{rr} values derived from experiments recorded at overpotentials in the anodic (+) and cathodic (−) Tafel regions can be used to calculate α values according to:

$$\alpha_{\pm} = \left(\frac{RT}{F}\right)\left(\frac{1}{j_s}\frac{1}{R_{rr}}\right)\Bigg|_{E=E_{rdx}\pm|\eta|} \quad (6)$$

where j_s represents the stationary current density for the redox couple in solution.

For the sake of comparison, kinetic parameters calculated from EIS and steady-state data are shown in Table 2. A satisfactory agreement between the two sets of values was obtained. In Table 2, j_o values are referred to the real electrode area and an average from the cathodic and the anodic values is presented for the results obtained from polarization curves.

Experimental results show that $\alpha_- > \alpha_+$, what points to an electron transfer with the conduction band. However, α_- and α_+ differ appreciably from the theoretical values 1 and 0, that can be expected for a simple mechanism involving the conduction band [34]. Consequently, it is possible to postulate the contribution of direct electron tunneling through the space charge into the conduction band.

Decreasing values of j_o and α_+ according to E_f can be related to decreasing values of N_D (see Table 1) and in agreement with the observations reported for passive films on Ti [35] and on Fe [24]. With increasing donor concentration, and hence with decreasing Debye-length, the space charge barrier becomes thinner and tunneling becomes more important.

One feature of the experimental polarization curves is not in line with the theory for direct electron tunneling through the space charge barrier, namely, the straight portions of the anodic and cathodic Tafel lines do not extrapolate to the same exchange current. This has been understood in terms of an additional contribution due to resonance tunneling [12]. Moreover, Tafel lines in Fig. 5, at high cathodic overpotentials, develop a curvature resembling the shoulders observed when the dominant tunneling mechanism varies from direct tunneling to resonance tunneling [36]. However, evidence presented here for a contribution of resonance tunneling is not conclusive.

Fig. 7 shows a schematic representation of the oxide/redox electrolyte interface at equilibrium and with applied anodic overpotential. The diagram corresponds to an oxide film formed at E_f = 0.4 V in 0.75 M $KHCO_3$ + 0.05 M K_2CO_3, pH 8.9. The calculated value for E_{fb} allows to locate the position of the conduction band edge at the surface, which is characterized by an energy level U_C^S. The corresponding energy level of the valence band at the surface U_V^S results from a band-gap width U_g = 3.5 eV, as reported for SnO_2 [8]. It is noteworthy that, a wide range of band gap values has been reported for anodic SnO_2 ranging from 2.6 to 3.7 eV and also that the apparent band gap value could be related to the degree of hydration of the oxide [37,38]. It can be observed that the occupied energy levels of the redox system overlap well with the conduction band, in accordance with the postulated participation of this band in the electron transfer. Direct

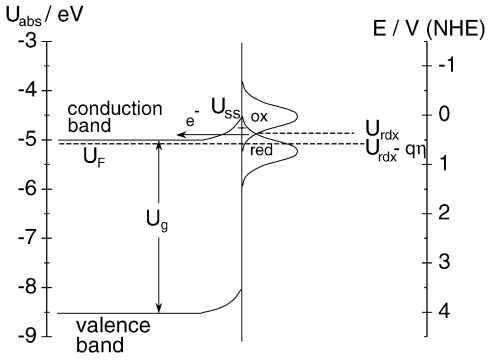

Fig. 7. Energy levels at the SnO_2/redox electrolyte interface for a passive film formed at E_f = 0.4 V, and with an anodic overpotential η applied. Scale in eV is referred to the energy of an electron at infinity, while scale in V is referred to the electrochemical potential of the hydrogen reference electrode under standard conditions (NHE). U_F corresponds to the Fermi energy of the oxide, and q represents the charge on the electron. Distribution function of surface states is centered at energy level U_{ss}. See text for definitions of the rest of the parameters in the figure.

electron tunneling through the space charge barrier, for small Debye-length conditions is also shown.

Impedance data indicate the presence of surface states with a distribution function centered at −0.1 V versus SCE (0.142 V versus NHE) and corresponding to an energy level U_{ss} = −4.64 eV. Even though a high concentration of surface states at U_{ss} might participate in the electron transfer, in order to dominate the current response, large $U_s^c - U_{rdx}$ values and an oxide with low N_D, are required [39]. Neither of these two conditions prevail in our experiments. Thus, electron transfer via surface states is considered to be negligible for the experimental conditions of this work.

4. Conclusions

Passive films grown on tin in carbonate-bicarbonate solution exhibit different types of electronic conduction, according to the formation potential. The different behavior is markedly dependent on the film thickness. While thin films (E_f < 0.4 V) behave as insulators, thicker films show *n*-type semiconduction. Localized states within the band gap are present, at least, at the surface.

Electron transfer between surface states and redox electrolyte does not contribute appreciably to the electronic current. Electron exchange with the film takes place with participation of the conduction band. Direct electron tunneling through the space charge barrier represents the most probable mechanism for these highly-doped passive films.

Acknowledgement

Drs. Gervasi and Vallejo are grateful to the Comisión de Investigaciones Científicas y Técnicas Buenos Aires for their research positions.

References

[1] Z. Galus, in: A.J. Bard (Ed.), Encyclopedia of Electrochemistry of the Elements, vol. I, Marcel Dekker, New York, 1973, p. 223.
[2] B.N. Stirrup, N.A. Hampson, Surf. Technol. 5 (1977) 429.
[3] P.E. Alvarez, S.B. Ribotta, M.E. Folquer, C.A. Gervasi, J.R. Vilche, Corros. Sci. 44 (2002) 49.
[4] M. Drogowska, H. Menard, L. Brossard, J. Appl. Electrochem. 21 (1991) 84.
[5] P. Schmuki, S. Virtanen, Electrochem. Soc. Interf. 6 (1997) 38.
[6] H. Tsuchiya, S. Fujimoto, O. Chihara, T. Shibata, Electrochim. Acta 47 (2002) 4357.
[7] Y.M. Zeng, J.L. Luo, P.R Norton, Thin Solid Films, 2004.
[8] A. Nanthakumar, N.R. Armstrong, in: H.O. Finklea (Ed.), Semiconductor Electrodes, Elsevier, Amsterdam, 1988, Chapter 4.
[9] S. Kapusta, N. Hackerman, Electrochim. Acta 25 (1980) 949.
[10] S. Kapusta, N. Hackerman, Electrochim. Acta 25 (1980) 1001.
[11] M. Metikoš-Huković, S. Omanović, A. Jukić, Electrochim. Acta 45 (1999) 977.
[12] W. Schmickler, J. Electroanal. Chem. Interf. Electrochem. 84 (1977) 203.
[13] S. Kapusta, N. Hackerman, J. Electrochem. Soc. 128 (1981) 327.
[14] C.Y. Chao, L.F. Lin, D.D. Macdonald, J. Electrochem. Soc. 129 (1982) 1874.
[15] D.D. Macdonald, S. Smedley, Electrochim. Acta 35 (1990) 1949.
[16] D.D. Macdonald, S.R. Biaggio, H. Song, J. Electrochem. Soc. 139 (1992) 170.
[17] E.B. Castro, Electrochim. Acta 39 (1994) 2117.
[18] A.T. Fromhold Jr., E.L. Cook, J. App. Phys. 38 (1967) 1546.
[19] C.A. Gervasi, P.E. Alvarez, Corros. Sci., in press.
[20] D.B. Bonham, M.E. Orazem, J. Electrochem. Soc. 139 (1992) 118.
[21] M. Anderman, J.H. Kennedy, in: H.O. Finklea (Ed.), Semiconductor Electrodes, Elsevier, Amsterdam, 1988, Chapter 3.
[22] C.A. Moina, F.E. Varela, L. Feria Hernández, F.O. Ybarra, J.R. Vilche, J. Electroanal. Chem. 427 (1997) 189.
[23] R.D. Lide (Ed.), Handbook of Chemistry and Physics, 73rd Edition, CRC Press, Boca Ratón, FL, 1993.
[24] U. Stimming, J.W. Schulze, Ber. Bunsenges. Phys. Chem. 80 (1976) 1297.
[25] S.U.M. Khan, W. Schmickler, J. Electroanal. Chem. 108 (1980) 329.
[26] V. Macagno, J.W. Schulze, J. Electroanal. Chem. 180 (1984) 157.
[27] S. Kapusta, N. Hackerman, Electrochim. Acta 25 (1980) 1625.
[28] D.B. Bonham, M.E. Orazem, AIChE J. 34 (1988) 465.
[29] M.P. Dare-Edwards, J.B. Goodenough, A. Hamnett, P.R. Travellick, J. Chem. Soc., Faraday Trans. 1 79 (1983) 2027.
[30] M.P. Dare-Edwards, A. Hamnett, P.R. Travellick, J. Chem. Soc., Faraday Trans. 1 79 (1983) 2111.
[31] M. Büchler, P. Schmuki, H. Böhni, T. Stenberg, T. Mäntylä, J. Electrochem. Soc. 145 (1998) 378.
[32] J.W. Schultze, in: R.P. Frankenthal, J. Kruger (Eds.), Passivity of Metals, The Electrochemical Society Inc, Princeton, New York, 1978, p. 82.
[33] E.B. Castro, J.R. Vilche, Electrochim. Acta 38 (1993) 1567–1572.
[34] F. Möllers, R. Memming, Ber. Bunsenges. Phys. Chem. 76 (1972) 469.
[35] K.E. Heusler, K.S. Yun, Electrochim. Acta 22 (1977) 977.
[36] W. Schmickler, J.W. Schulze, J. O'M Bockris, in: B.E. Conway, R.A. White (Eds.), Modern Aspects of Electrochemistry, vol. 17, Plenum, New York, 1986, pp. 357–410.
[37] F. Di Quarto, C. Sunseri, S. Piazza, M.C. Romano, J. Phys. Chem. B 101 (1997) 2519.
[38] S. Piazza, M. Santamaria, C. Sunseri, F. Di Quarto, Electrochim. Acta 48 (2003) 1105.
[39] D. Vanmaekelbergh, Electrochim. Acta 42 (1997) 1121.